https://doi.org/10.1007/s41230-021-0023-0



# Shear bands of as-cast and semi-solid $Ti_{48}Zr_{27}Cu_6Nb_5Be_{14}$ bulk metallic glass matrix composites

**Xin-hua Huang[1, 2, 4], Lin-hao Zhu[2, 3], Hong-min Guo[2, 3], Hua-lan Jin[2, 3], *Xiang-jie Yang[1, 2]**

*1. School of Mechanical and Electrical Engineering, Nanchang University, Nanchang 330031, China*

*2. Key Laboratory of Near Net Forming in Jiangxi Province, Nanchang University, Nanchang 330031, China*

*3. School of Material Science and Engineering, Nanchang University, Nanchang 330031, China*

*4. Hunan Province Special Equipment Inspection and Research Institute, Changsha 410117, China*

**Abstract:** The as-cast $Ti_{48}Zr_{27}Cu_6Nb_5Be_{14}$ bulk metallic glass matrix composites (BMGMCs) were fabricated using a copper mold suction casting method. Then, the semi-solid BMGMC samples were obtained following an isothermal treatment (heating at 900 °C for 10 min, then cooling with water). The microstructure and compression property were investigated by scanning electronic microscopy (SEM) and universal mechanical tester. As a result of the isothermal treatment, the crystal shapes change from fine, granular, and dendritic to spherical or vermicular, and the average crystal size of the as-cast and semi-solid samples is 2.2 μm and 18.1 μm, respectively. The plasticity increases from 5.31% in the as-cast to 10.23% in the semi-solid samples, with an increase of 92.66%. The shear bands from different areas of the side surfaces of as-cast and semi-solid compression fracture samples were observed. The characteristic changes of multiplicity, bend, branch and intersection of shear bands in different areas indicate that the deformation of as-cast and semi-solid samples is non-uniform during compression. It is found that poor plasticity of the as-cast samples or good plasticity of the semi-solid samples are reflected by characteristics of the shear bands. The semi-solid isothermal treatment improves the plasticity by forming large crystals which can block the expansion of shear bands and promote the multiplicity of shear bands.

**Key words:** shear bands; $Ti_{48}Zr_{27}Cu_6Nb_5Be_{14}$; as-cast; semi-solid; plasticity

**CLC numbers:** TG146.23 **Document code:** A **Article ID:** 1672-6421(2021)01-075-08

## 1 Introduction

Bulk metallic glass matrix composites (BMGMCs) are similar to bulk metallic glass materials, and also have many advantages, including high elastic strain limit, high strength, good conductivity, and high magnetic permeability [1-3]. They have been widely used as semiconductors, superconductors, transformers, and other high magnetic permeability materials [4-6]. However, a fatal disadvantage of BMGMCs is poor plasticity, which can cause brittle fracture. This weakness has greatly limited their application in the field of engineering [7-9]. Therefore, ways to improve the plasticity of BMGMCs has become an interesting topic in recent years.

In the 1970s, Turnbull D revealed that the formation of the shear bands meant the occurrence of plastic deformation of amorphous alloys, and the deformation was concentrated in the local areas around the shear bands [10]. By studying the relationship between shear band characteristics and the plasticity of BMGMCs [11-13], it was found that the plasticity was improved effectively as the quantity of shear band increased. It was also found that a single shear band would easily lead to brittle fracture with very low plasticity, while multiple shear bands could enhance the plasticity [14]. Studying the effects of shear band spacing on the plasticity showed a narrow shear band average spacing in samples with good plasticity [15, 16]. There is a general law that the BMGMC would have perfect plasticity if the shear bands have complex characteristics such as multiple shear bands, a high density of shear bands, and narrow distances between the shear bands.

Plasticity is not only related to the characteristics

***Xiang-jie Yang**

Male, Ph. D, Professor. Research interests: amorphous alloys and semi-solid precise material forming. He has been responsible for four National Natural Science Foundation Programs and one program through the Ministry of Science and Technology, obtained 15 invention patents and 10 utility model patents. To date, he has published more than 70 academic papers.

E-mail: yangxj@ncu.edu.cn;

**Received: 2020-05-12; Accepted: 2020-11-16**

of the shear bands, but also to the movements of the shear bands. Hays et al. [17] found that crystals with good toughness easily initiated the shear bands and promoted the shear bands to multiplicity. Qin et al. [18] studied Cu-based BMGMC and found that the ductile dendrites deflected the shear band propagating direction, resulting in shear band branching, which improved plasticity. Larger crystals were also found to affect the movements of shear bands, for example, blocking the expansion of shear bands, promoting shear band multiplicity, intersecting shear bands in different directions, inducing the branching of the shear bands, forcing the shear bands to bend, and causing the expansion directions to shift [19-23]. The relationship between the content of the crystal phase and shear bands in BMGMCs showed that as the crystal content increased, the shear bands underwent some of the movements mentioned above [24]. The toughness of crystals, crystal size, and content of crystal play an important role in affecting the properties of the shear bands, which in turn affect the plasticity of the BMGMCs.

Based on the fact that semi-solid isothermal treatment could greatly improve the plasticity of traditional metal materials, this study explored whether this method would have the same effect on $Ti_{48}Zr_{27}Cu_6Nb_5Be_{14}$ BMGMCs. The characteristics and movements of shear bands in different regions of fractured samples were observed to study the plasticity of as-cast and semi-solid samples. These characteristics were used to explore the mechanisms of non-uniform deformation and how semi-solid isothermal treatment improved the plasticity of BMGMCs.

## 2 Experimental procedure

Ti, Zr, Nb, Cu, and Be with purity greater than 99.995% were mixed and melted in argon atmosphere by arc melting to prepare ingots with the composition of $Ti_{48}Zr_{27}Cu_6Nb_5Be_{14}$, configured according to atomic ratio. The ingots were melted 4–5 times to ensure chemical homogeneity and then cast into a water-cooled copper mold to obtain as-cast $Ti_{48}Zr_{27}Cu_6Nb_5Be_{14}$ samples with a diameter of 4 mm and a length of 70 mm.

For the semi-solid $Ti_{48}Zr_{27}Cu_6Nb_5Be_{14}$ samples, first, the as-cast $Ti_{48}Zr_{27}Cu_6Nb_5Be_{14}$ samples were vacuum encapsulated inside quartz tubes to avoid high temperature oxidation. Second, an electric furnace (YFFG40/13G-YC) was heated to 900 °C in advance, and the encapsulated as-cast $Ti_{48}Zr_{27}Cu_6Nb_5Be_{14}$ samples were put into the electric furnace. Lastly, these samples were kept at 900 °C for 10 min, and then were water quenched, obtaining the semi-solid samples.

The phase constitution was tested by X-ray diffraction (XRD) with Cu Kα radiation. The microstructure was observed by scanning electronic microscopy (SEM), and the compositions of the crystals were tested by energy dispersive spectroscopy (EDS). Room temperature uniaxial compressive tests were completed by an universal mechanical tester (Instron 5582) at the rate of $5\times10^{-6}$ $s^{-1}$. Compression samples were prepared from the middle of as-cast and semi-solid samples, 4 mm in diameter and 7 mm in length. The upper and lower surfaces of the compression samples were polished to make them parallel to each other and perpendicular to the loading direction.

Image-Pro Plus V6.0 (IPP) software was used to identify the crystals and amorphous matrix in the metallographic images as different colors. The crystals were recognized according to the color. Volume fractions and the number of crystals were determined by IPP, and the area of each crystal was measured using the IPP program. Then, the average crystal size $D$ was calculated according to the following Eq. (1) [25]:

$$D = \frac{\sum_{i=1}^{N}\sqrt{4A_i/\pi}}{N} \quad (1)$$

where $A_i$ is the area of the $i$th crystal and $N$ is the total number of crystals that are counted.

## 3 Results

### 3.1 Microstructure and plasticity

Figure 1 shows the SEM micrographs of the as-cast and semi-solid samples. The crystal phase volume fractions of as-cast and semi-solid samples of $Ti_{48}Zr_{27}Cu_6Nb_5Be_{14}$ are 62.3% and 58.4%, respectively. The numerators of Eq. (1) corresponding to the as-cast and semi-solid samples are 1,347.7 μm and 4,312.8 μm, and the corresponding values of the denominator $N$ are 609 and 238, respectively. Therefore, the average grain sizes are 2.2 μm and 18.1 μm for the as-cast and semi-solid samples, respectively. This means that the crystal sizes are greatly increased following the isothermal treatment. The crystal shapes change from fine, granular, and dendritic to spherical or vermicular. The EDS results of crystal of the as-cast and semi-solid samples at the white point in the top right corner of the micrographs are shown in Fig. 2. Table 1 provides the element content of these samples determined by EDS. The Ti, Zr, Cu and Nb element content of the as-cast crystal is 58.50wt.%, 29.28wt.%, 5.42wt.% and 6.80wt.%, respectively, and in the semi-solid crystal is 62.93wt.%, 26.37wt.%, 2.08wt.% and 8.62wt.%, respectively. Table 1 shows that the Ti and Nb contents in the crystals increase after isothermal treatment, replacing part of the Cu and Zr due to atomic diffusion, and Be is not dissolved in the crystals, which is consistent with a previous study [26]. XRD spectra (Fig. 3) shows that the crystal phases of the as-cast and semi-solid samples are both bcc β-Ti phase, indicating that the semi-solid isothermal treatment does not cause a phase transition.

Stress-strain curves of the as-cast and semi-solid samples obtained by compression testing are shown in Fig. 4. The compressive plasticity of as-cast and semi-solid samples at ambient temperature, $\varepsilon_{as\text{-}cast}$ and $\varepsilon_{semi\text{-}solid}$, is 5.31% and 10.23%, respectively. This means that the plasticity is improved by 92.66% after isothermal treatment, and also shows that the isothermal treatment contributes to improving the plasticity of $Ti_{48}Zr_{27}Cu_6Nb_5Be_{14}$.

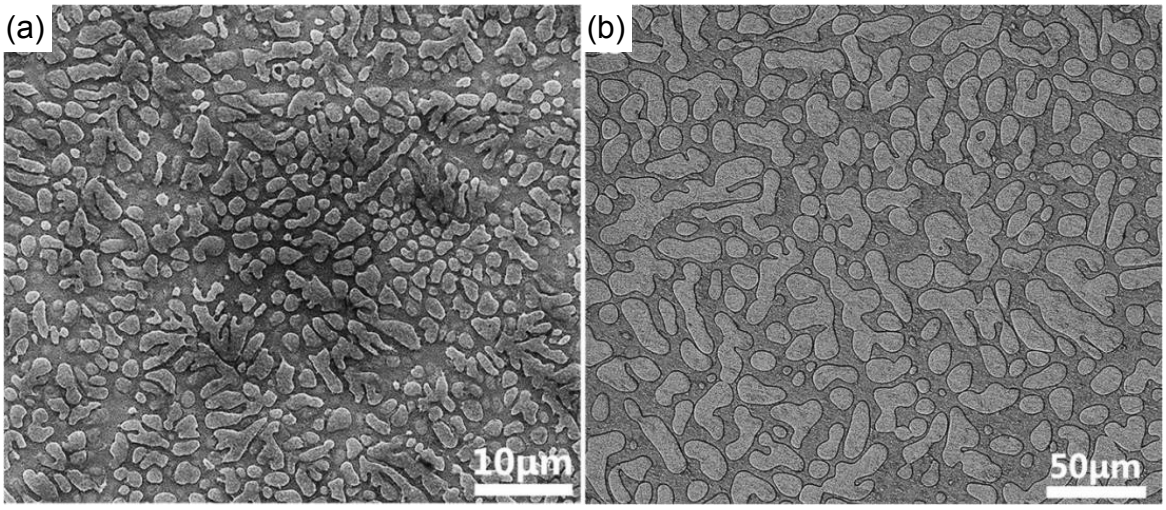


Fig. 1: Structure characteristics of $Ti_{48}Zr_{27}Cu_6Nb_5Be_{14}$: (a) as-cast sample; (b) semi-solid sample

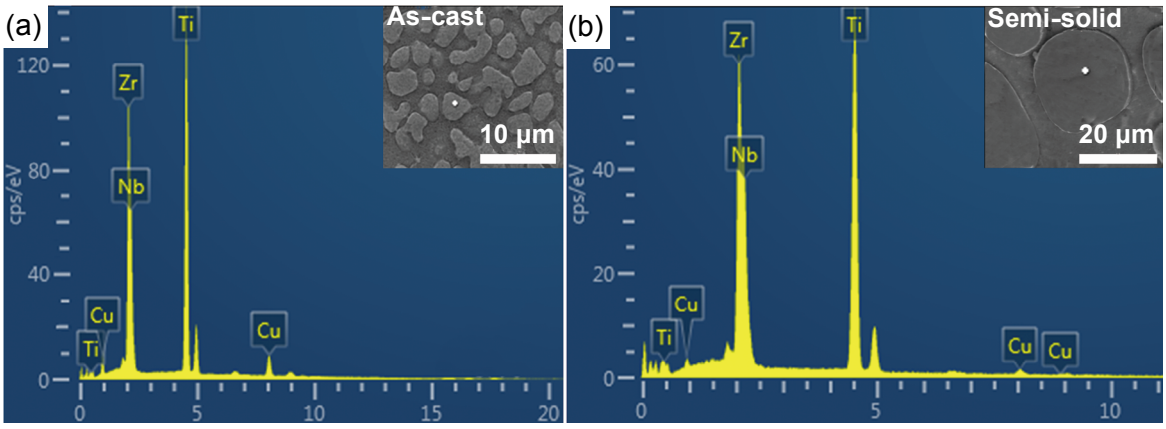


Fig. 2: Results of EDS corresponding to scanning white points shown in top right corner micrographs: (a) EDS of as-cast crystal; (b) EDS of semi-solid crystal

Table 2: Element contents of as-cast and semi-solid crystals, corresponding to EDS measurements in Figs. 2(a) and 2(b) (wt.%)

| Sample | Ti | Zr | Cu | Nb |
|---|---|---|---|---|
| As-cast | 58.50 | 29.28 | 5.42 | 6.80 |
| Semi-solid | 62.93 | 26.37 | 2.08 | 8.62 |

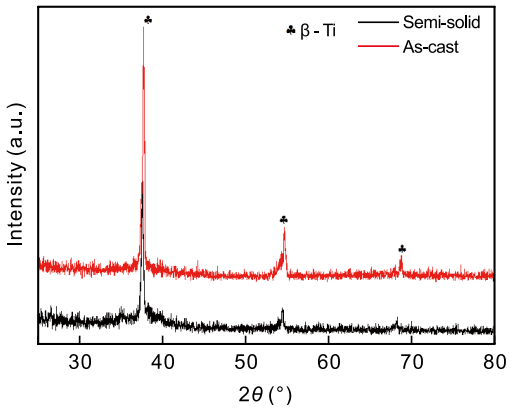


Fig. 3: XRD spectra of as-cast and semi-solid $Ti_{48}Zr_{27}Cu_6Nb_5Be_{14}$ samples

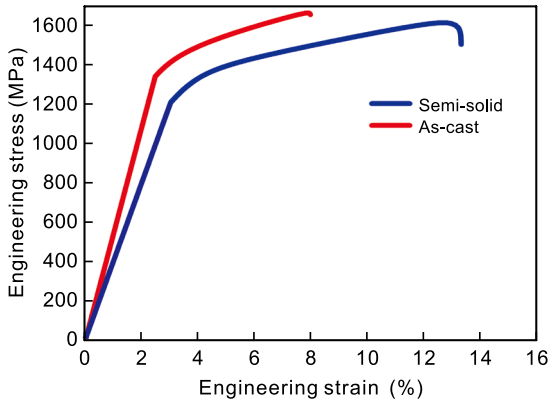


Fig. 4: Compressive stress-strain curves of as-cast and semi-solid $Ti_{48}Zr_{27}Cu_6Nb_5Be_{14}$ samples

## 3.2 Shear band characteristics

Figure 5 shows a schematic of shear band observation area on the side surface of the compression fracture $Ti_{48}Zr_{27}Cu_6Nb_5Be_{14}$ specimens. As-cast and semi-solid samples are shown in blue and yellow, respectively. In Fig. 5, the side surface regions a-d and A-D of the as-cast and semi-solid fracture samples are selected to observe the shear bands respectively, and the plasticity of as-cast and semi-solid samples was studied.

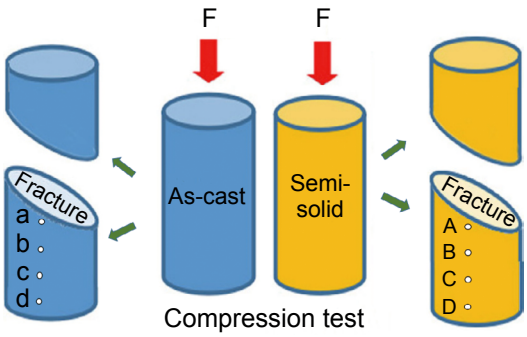


**Fig. 5: Schematic of shear band observation area on side surface of compression fracture specimens**

Figure 6 shows SEM micrographs of the side surface morphology (corresponding to a-d areas in Fig. 5) of fractured as-cast $Ti_{48}Zr_{27}Cu_6Nb_5Be_{14}$ sample. In Area a, there are very clear approximately parallel shear bands along the shear stress direction and shear bands expanding straightly through the crystals and amorphous matrix. The length of shear band expansion is great, as shown in Fig. 6(a). The shear bands penetrate the crystals along a straight line, as shown in Fig. 6(I), which is a local enlarged image of the red boxed area I in Fig. 6(a). Compared with Area a, Area b has fewer shear bands and the visibility of shear bands is weakened, as shown in Fig. 6(b). The shear bands of Area c are unapparent. In addition, the quantity of shear bands is less than in either Areas a or b, as shown in Fig. 6(c). There are nearly no shear bands in Area d, as shown in Fig. 6(d). As the as-cast sample, when the local area is far away from the fracture surface (i.e., from Area a to Area d), it can be inferred that the shear bands spacing enlarges by degree, shear band length decreases gradually, and the shear band gradually becomes unobvious and eventually disappears.

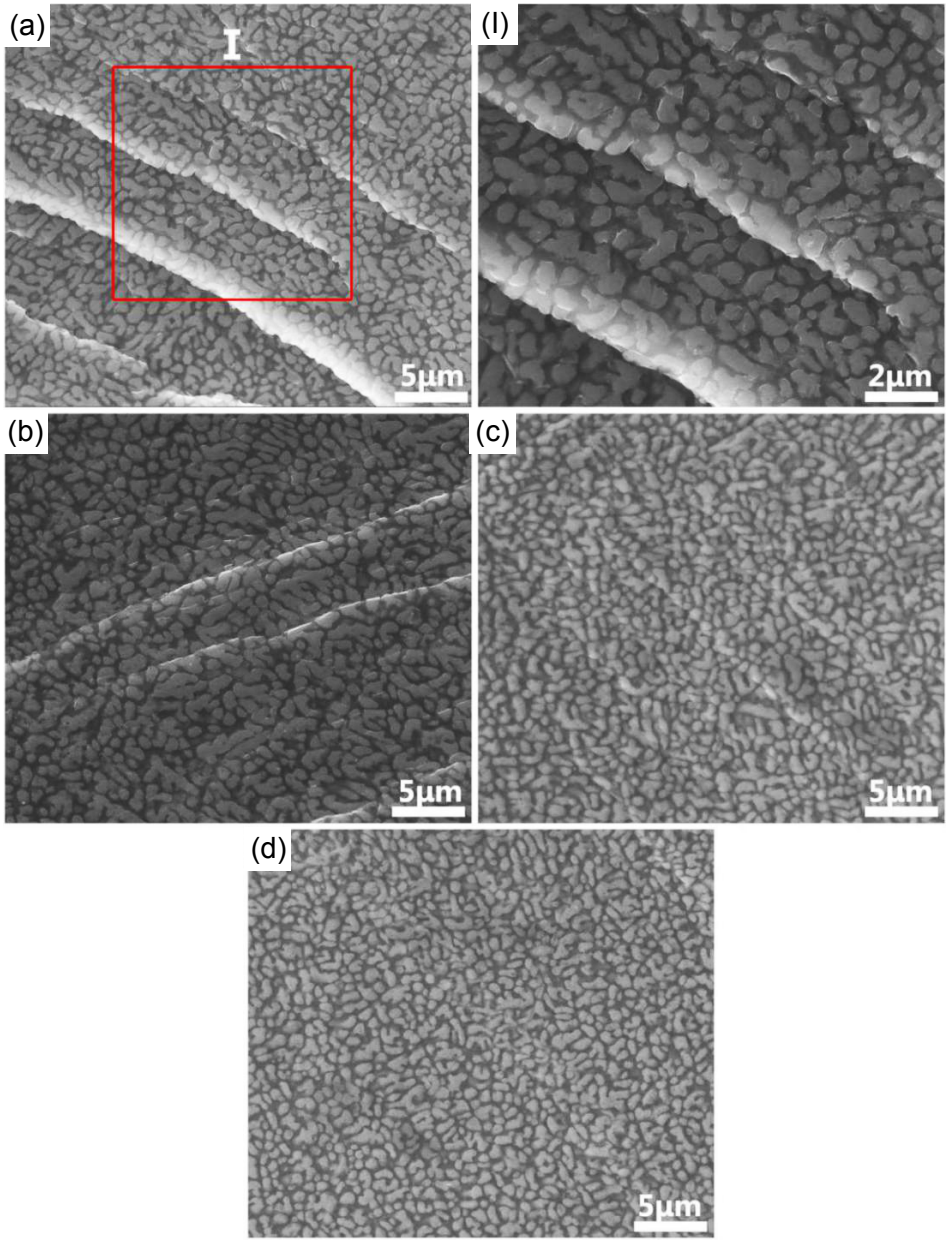


**Fig. 6: Side surface shear band morphology of a fractured as-cast $Ti_{48}Zr_{27}Cu_6Nb_5Be_{14}$ sample, (a), (b), (c), and (d) represent Areas a, b, c, and d shown in Fig. 5, respectively**

Figure 7 shows SEM micrographs of the lateral morphology (corresponding to Areas A-D in Fig. 5) of a semi-solid $Ti_{48}Zr_{27}Cu_6Nb_5Be_{14}$ sample. As shown in Fig. 7(a), the shear bands have more distinct features, such as a very large number of shear bands, high density, and narrow shear band spacing inside the crystals compared with the amorphous matrix. The expansions of shear bands are blocked and terminated within the crystals, so that the lengths of shear bands are short, and the expansion directions of shear band are shifted. The shear bands are multiplied and bent. The shear bands are found along different directions and some of them even cross, as shown by the blue and white arrows in Fig. 7(I), which is a partial enlargement of the red boxed area in Fig. 7(a).

There are also a large number of shear bands in Area B, corresponding to Fig. 7(b). Some of the shear bands along different directions cross, similar to Area A. However, the number of shear bands noticeably decreases compared with Area A, and the shear band spacing is larger than that in Area A. Movements of the shear bands including bending, intersecting of shear bands in different directions, and multiplying, are present in Area B, but are not as obvious as in Area A.

Figure 7(c) shows that the shear bands of Area C only exist in the crystals and the distribution is sparse. The number of shear bands is further reduced, comparing with Figs. 7(a) and (b). The biggest feature of Area C is that no shear band is found in the amorphous matrix. This suggests that the shear bands firstly form in the crystals and then extend into the amorphous matrix. In Area D, no shear bands are observed in either the crystals or the amorphous matrix, as shown in Fig. 7(d). In all, for the semi-solid sample, from Areas A to D, the shear band characteristics show three main changes: (1) the number of shear bands gradually reduces to almost zero; (2) the offset of the expansion direction of shear bands becomes less and less obvious; (3) multiplying, bending, branching and intersecting of shear bands become weaker and then almost disappear.

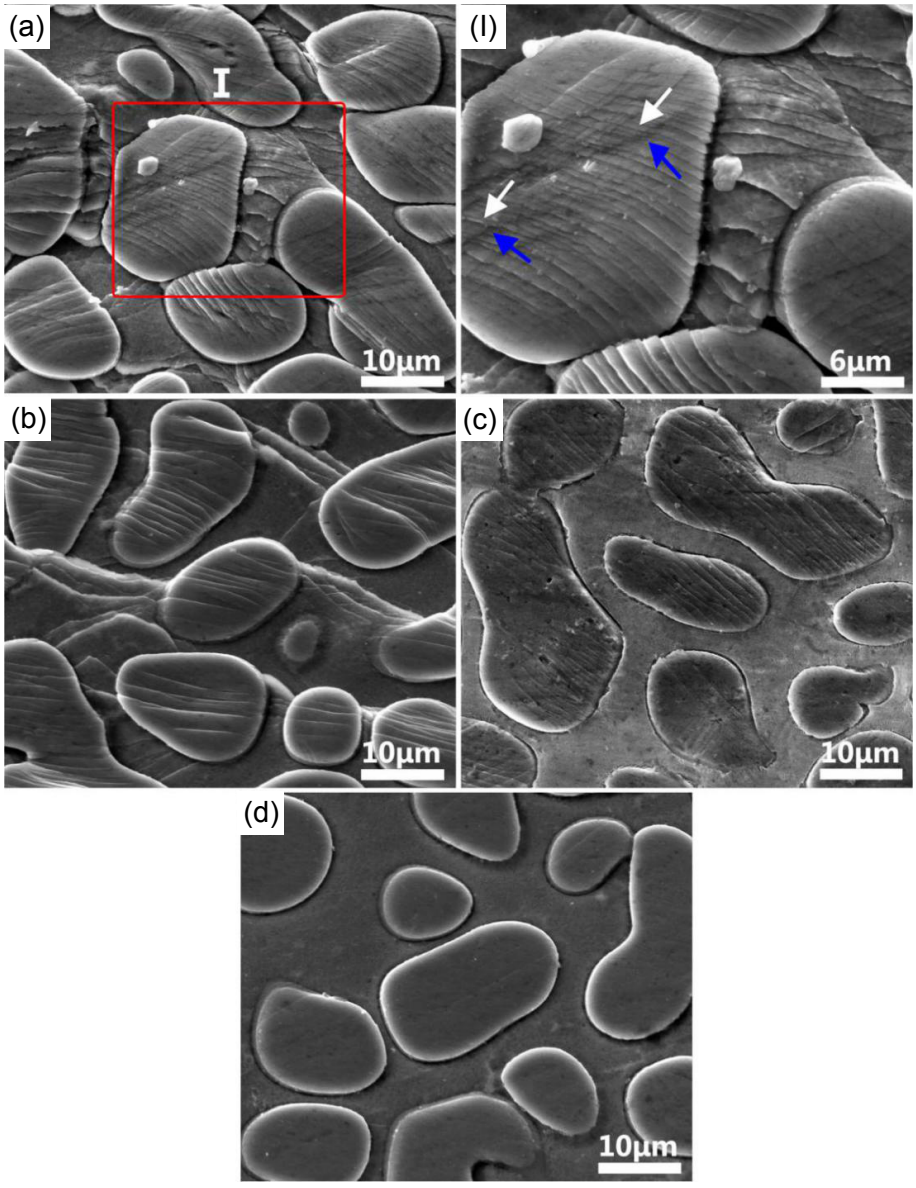


**Fig. 7: Lateral surface shear band morphology of a fractured semi-solid $Ti_{48}Zr27Cu_6Nb_5Be_{14}$ sample, (a), (b), (c), and (d) represent Areas A, B, C, and D shown in Fig. 5, respectively**

# 4 Discussion and analysis

## 4.1 Local strain and stress

Since the characteristics of shear bands can reflect plasticity, and the plasticity is the comprehensive reflection of countless local plasticity, the local plasticity was analyzed in combination with the change characteristics of these shear bands from Areas a-d or A-D mentioned in Section 3 to obtain the relationship between shear bands and plasticity.

$\varepsilon_a$, $\varepsilon_b$, $\varepsilon_c$ and $\varepsilon_d$ are defined as the local plastic strain of Areas a, b, c, and d in the as-cast samples, respectively. In the same way, $\varepsilon_A$, $\varepsilon_B$, $\varepsilon_C$, and $\varepsilon_D$ are defined as the local plastic strain of Areas A, B, C, and D in the semi-solid samples, respectively. $\varepsilon_{as\text{-}cast}$ and $\varepsilon_{semi\text{-}solid}$ are defined as the global plastic strains of as-cast and semi-solid samples, respectively. According to the shear band characteristics, it could be inferred that $\varepsilon_a > \varepsilon_b > \varepsilon_c > \varepsilon_d$ and $\varepsilon_A > \varepsilon_B > \varepsilon_C > \varepsilon_D$. This shows that the plastic deformation of the as-cast and semi-solid samples is non-uniform. Similarly, the relationship of the plastic strains in local regions corresponding to as-cast and semi-solid samples is $\varepsilon_A > \varepsilon_a$, $\varepsilon_B > \varepsilon_b$ and $\varepsilon_C > \varepsilon_c$, which shows why the global plastic strain $\varepsilon_{semi\text{-}solid} > \varepsilon_{as\text{-}cast}$.

The shear band characteristics in different areas of the fracture sample are different, and the generation of shear band is related to stress. Therefore, it is necessary to explore the relationship between stress and shear bands. The generation of shear bands is a significant manifestation of plastic strain and also marks the yield strength of the local area. The crystals and amorphous matrix are different phases, so it is logical that their yield strengths are different.

For the semi-solid samples, $\sigma_{crystal}$ is defined as the yield strength of the crystal phase and $\sigma_{matrix}$ is the yield strength of the amorphous matrix. $\sigma$ is defined as the stress in the process of compression loading. First, suppose $\sigma_{matrix} < \sigma_{crystal}$. During compression loading, the stress $\sigma$ increases gradually. When $\sigma_{matrix} < \sigma < \sigma_{crystal}$, the amorphous matrix yields first, and the shear bands form in the amorphous matrix. However, Figure 7(c) shows that the amorphous matrix has no shear bands, while the crystals have shear bands. It could be deduced that the amorphous matrix does not yield and it is still in the elastic deformation stage, while the crystal has already yielded, resulting in plastic deformation. This means that the crystals are easier and earlier to yield than the amorphous matrix. The supposition is contrary to the actual result, so the relationship is actually $\sigma_{crystal} < \sigma_{matrix}$.

When the local stress $\sigma < \sigma_{crystal}$, it is implied that no shear bands are formed in either the crystal or the amorphous matrix, in accordance with Fig. 7(d). When $\sigma_{crystal} < \sigma < \sigma_{matrix}$, shear bands form in the crystals, and no shear bands in the amorphous matrix, consistent with Fig. 7(c). When $\sigma > \sigma_{matrix}$, shear bands are generated in both the crystal and amorphous matrix, reflected in Fig. 7(b). When $\sigma >> \sigma_{matrix}$, the shear bands are observed both in the crystals and amorphous matrix, and the shear band characteristics and movements are very complex, as shown in Fig. 7(a). If $\sigma_A$, $\sigma_B$, $\sigma_C$ and $\sigma_D$ are defined as local stresses of Areas A, B, C and D, respectively, the relationship between the local stress and yield strengths is $\sigma_A > \sigma_B > \sigma_{matrix} > \sigma_C > \sigma_{crystal} > \sigma_D$. From the above analysis, Area A of the semi-solid samples, which is closest to the fracture area, has greater stress and its plastic deformation is greater than other areas.

For as-cast samples, $\sigma_a$, $\sigma_b$, $\sigma_c$ and $\sigma_d$ are defined as local stress of Areas a, b, c and d, respectively. Their shear bands characteristics are simple and the relationship between $\sigma_{matrix}$ and $\sigma_{crystal}$ of the as-cast samples could not be inferred. But the relationship $\sigma_a > \sigma_b > \sigma_c > \sigma_d$ could be still determined according to shear band characteristics. This shows that the local stresses of as-cast and semi-solid samples are uneven distributions.

## 4.2 Analysis of shear band expansion

The expansion ability of the shear band is related to its own energy, and high energy means strong expansion ability. Usually, the energy is mainly estimated by the temperature of the shear bands, as shown in Eq. (2) [27]:

$$\Delta H = \Delta T_{centre} \rho c \sqrt{\pi \alpha t} \tag{2}$$

where $\Delta H$ is the energy contained in the shear band, $\Delta T_{centre}$ is the difference between the core temperature of a single shear band and the ambient temperature, $\rho$ is the material density, $c$ is the specific heat, $\alpha$ is the thermal diffusion coefficient, and $t$ is the shearing duration time. The chemical compositions of the as-cast and semi-solid samples are similar, so the parameters are unchanged, except for $\Delta T_{centre}$. As the number of shear bands in the as-cast sample is far less than that of the semi-solid sample, and when the total temperature rise of the sample is constant during compression, the temperature rise ($\Delta T_{centre}$) of each shear band in the as-cast sample is much greater than that of the semi-solid sample, which means that the $\Delta H$ of Area A is less than in Area a for a shear band. Therefore, the single shear band in the as-cast samples has stronger expansion ability due to having more energy than those in the semi-solid samples, so that the former could expand a longer length than the latter. This is one of the reasons why the shear bands of as-cast samples expand larger lengths than semi-solid samples. In addition to expansion ability, the extension lengths of the shear bands are also related to the crystal sizes and spacing, and their effects on the extension lengths of the shear bands will be discussed next.

In the semi-solid samples, the crystal sizes are large, and the shear bands cannot bypass these crystals to expand. So, when these crystals are inevitably passed through, the expansion would encounter great obstacles, causing the expansion to be forced to stop in these crystals. Thus the extension lengths of the shear band are small. Another point is that, for the as-cast samples, the crystals can't hinder the expansion of shear bands and are passed through, as shown by the blue arrows in Fig. 8(a), and fine crystals are bypassed along their edges, as shown by the white arrows in Fig. 8(b) (I, II, III, IV) in the corresponding red boxed areas (I, II, III and IV) in Fig. 8(a).

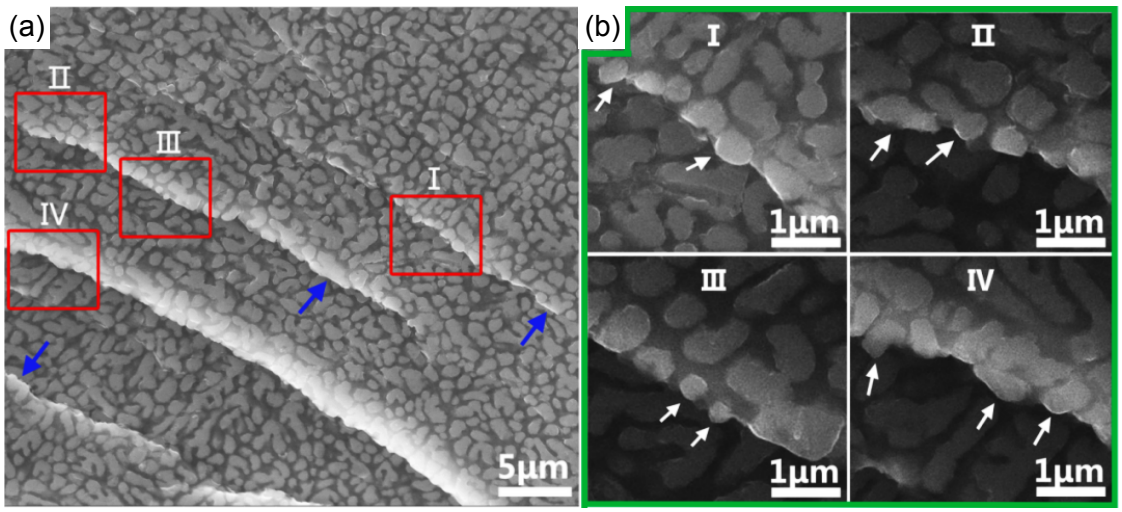


**Fig. 8: Lateral surface shear band morphology of Area a (a), and enlarged views (I, II, III, IV) (b) of red boxed areas in (a), which show that shear bands could bypass fine crystals and continue to expand**

This indicates that the expansion lengths of the shear bands are large because the crystals cannot actively prevent the expansion of the shear bands.

In order to learn more about the relationship between the lengths of the shear bands in the as-cast and semi-solid samples, Figure 9 was created. Figure 9 is a schematic diagram of shear bands passing through large crystals and bypassing fine crystals. Red lines represent the shear bands, blue circles represent the large crystals of semi-solid samples and yellow circles represent the crystals of as-cast samples. $D$ and $d$ are defined as the average crystal sizes of the as-cast sample and the semi-solid samples, respectively. $\gamma$ is defined as the average crystal spacing.

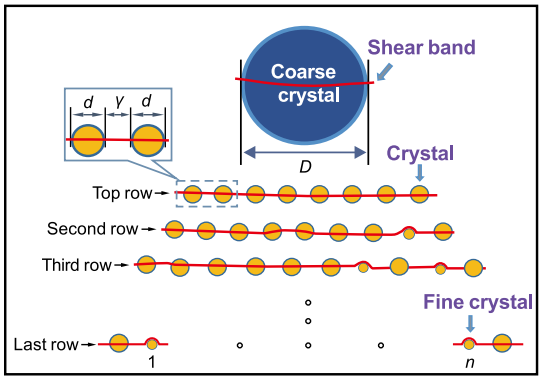


**Fig. 9: Schematic diagram of shear bands passing through large crystals and bypassing fine crystals**

As the crystals of the $Ti_{48}Zr_{27}Cu_6Nb_5Be_{14}$ are bcc β-Ti before and after the semi-solid isothermal treatment, it is proposed that the energy consumed by the extension of the shear bands through the unit length of the semi-solid crystals is approximate to that of the as-cast crystals. The energy consumption of the shear bands mainly depends on crystal size and quantity. According to the average crystal size, one crystal of the semi-solid sample is equivalent to eight crystals of the as-cast sample. The amorphous matrix is a brittle phase and consumes only a tiny bit of energy when the shear bands pass though the matrix. This explains why there is unlimited extension of the shear bands in the amorphous matrix. The energy consumed by the extension of the shear bands in the amorphous matrix can be ignored.

The relationship between the shear band lengths of as-cast and semi-solid samples was also analyzed. $L_1$ and $L_2$ are defined as the lengths of the shear bands, which pass through one large crystal of the semi-solid sample and eight crystals of the as-cast sample, respectively. $L_1 = D \approx 8d$.

The parameter $\gamma$ represents average crystal spacing of as-cast samples and $n$ represents the number of fine crystals. When there are no fine crystals, $L_2 = 8d + 7\gamma$, as shown in the top row in Fig. 9. When there is one fine crystal, $L_2 = 8d + 8\gamma$ (second row in Fig. 9). When there are two fine crystals, $L_2 = 8d + 9\gamma$ (third row in Fig. 9). When there are $n$ fine crystals, $L_2 = 8d + (7 + n)\gamma \approx L_1 + (7 + n)\gamma$ (last row in Fig. 9). These examples show that $L_2 > L_1$ and when $n$ is very large, $L_2 >> L_1$.

In summary, the shear bands of as-cast samples expand along straight lines by passing through crystals and bypassing fine crystals, so that extension lengths are fairly long. These factors easily result in the infinite expansion of the shear bands, which eventually lead to brittle fracture in the as-cast samples. This reveals the mechanism behind the poor plasticity of as-cast BMGMCs. Another point is that the initiation of shear bands in the crystals is mainly attributed to dislocations because dislocations transform into shear bands under stress [28]. When the dislocation density is the same, the large crystals of semi-solid samples have a greater number of dislocations than the crystals of as-cast samples, so the large crystals could form a greater number of shear bands than general crystals. A great number of shear bands are one of the reasons for the increase of plasticity. In addition, the large crystals affect the shear band movements, such as hindering the expansion to promote the shear bands multiplication, branching and bending. These several factors indicate that semi-solid samples have better plasticity because of the large crystals. Accordingly, it reveals that the mechanism behind increasing the plasticity of the semi-solid isothermal treatment is to form large crystals.

## 5 Conclusions

(1) The average grain sizes of the as-cast and semi-solid samples are 2.2 μm and 18.1 μm, respectively. The semi-solid isothermal treatment does not cause a phase transition, the crystal phases of the as-cast and semi-solid samples are both bcc β-Ti phase .

(2) Shear band characteristics in different areas reveal the mechanisms of inhomogeneous deformation and uneven stress distribution in $Ti_{48}Zr_{27}Cu_6Nb_5Be_{14}$ during compression. As the distance from the fracture point increases, local stress and plastic deformation gradually decrease.

(3) Shear bands of the as-cast samples pass through or bypass the crystals, and the crystals cannnot actively block the expansion of the shear bands, which leads the shear bands to have the characteristics of small number, instability expansion, long length and expansion along straight line, and so on, resulting in brittle fracture, and the plasticity is only 5.31%.

(4) Semi-solid isothermal treatment substantially enhances the plasticity, up to 10.23%, of BMGMCs by forming large crystals, which play an important role in creating abundant shear band characteristics, such as large number, multiplicity, bend, branch, and intersection of shear bands.

## Acknowledgements

This research was supported by the National Natural Science Foundation of China (Nos.: 51674144, 11364031), the Luodi Research Plan of Jiangxi Educational Department (No.: KJLD14016), the Nature Science Foundation of Jiangxi Province (Nos.: 20122BAB206021, 20133ACB21003), and the Jiangxi Province Young Scientists Cultivating Programs (No.: 20122BCB23001).

## References

[1] Greer A L. Metallic glasses. Science, 1995, 267(5206): 1947–1953.
[2] Dmitri V, Louzguine L, Akihisa I. Bulk metallic glasses: Formation, structure, properties and applications. Handbook of Magnetic Materials, 2013, 21: 131–171.
[3] Johnson W L. Bulk glass-forming metallic alloys: Science and technology. MRS Bulletin, 1999, 24(10): 42–56.
[4] Zeng Q S, Sheng H W, Ding Y, et al. Long-range topological order in metallic glass. Science, 2011, 332(6036): 1404–1406.
[5] Cheng Y Q, Ma E. Atomic-level structure and structure property relationship in metallic glasses. Progress in Materials Science, 2011, 56(4): 379–473.
[6] Na J H, Demetriou M D, Floyd M, et al. Compositional landscape for glass formation in metal alloys. Proceedings of the National Academy of Sciences, 2014, 111(25): 9031–9036.
[7] Ma E. Tuning order in disorder. Nature Materials, 2015, 14(6): 547–552.
[8] Johnson W L, Na J H, Demetriou M D. Quantifying the origin of metallic glass formation. Nature Communications, 2016, 7: 10313.
[9] Masumoto T, Murata T. Deformation of amorphous metals. Materials Science and Engineering, 1976, 25: 71–75.
[10] Turnbull D, Cohen M H. On the free volume model of liquid glass transition. The Journal of Chemical Physics, 1970, 52(6): 3038–3041.
[11] Spaepen F. A microscopic mechanism for steady state inhomogeneous flow in metallic glasses. Acta Metallurgica, 1977, 25(4): 407–415.
[12] Shete M K, Singh I, Narasimhan R, et al. Effect of strain hardening and volume fraction of crystalline phase on strength and ductility of bulk metallic glass composites. Scripta Materialia, 2016, 124: 51–55.
[13] Zhai H M, Xu Y H, Zhang F, et al. Effect of transition metal elements (Cu, Ni, Co and Fe) on the mechanical properties of Ti-based bulk metallic glass composites. Journal of Alloys and Compounds, 2017, 694: 1–9.
[14] Jiang F, Jiang M Q, Wang H F, et al. Shear transformation zone volume determining ductile-brittle transition of bulk metallic glasses. Acta Materialia, 2011, 59(5): 2057–2068.
[15] Fan C, Li H Q, Kecskes L J, et al. Mechanical behavior of bulk amorphous alloys reinforced by ductile particles at cryogenic temperatures. Physical Review letters, 2006, 96(14): 145506.
[16] Lee M L, Li Y, Schuh C A. Effect of a controlled volume fraction of dendritic phases on tensile and compressive ductility in La-based metallic glass matrix composites. Acta Materialia, 2004, 52(14): 4121–4131.
[17] Hays C C, Kim C P, Johnson W L. Microstructure controlled shear band pattern formation and enhanced plasticity of bulk metallic glasses containing in situ formed ductile phase dendrite dispersions. Physical Review Letter, 2000, 84(13): 2901–2904.
[18] Qin C L, Zhang W, Katsuhiko A. A novel Cu-based BMG composite with high corrosion resistance and excellent mechanical properties. Acta Materialia, 2006, 54(14): 3713–3719.
[19] Zan B, Hidemi K, Qin C L, et al. Cu-Hf-Ti-Ag-Ta bulk metallic glass composites and their properties. Acta Materialia, 2005, 53(7): 2037–2048.
[20] Sun X H, Wang Y S, Fan J, et al. Plasticity improvement for dendrite/metallic glass matrix composites by pre-deformation. Materal and Design, 2015, 86: 266–271.
[21] Wu R F, Jiao Z M, Wang Y S, et al. Excellent plasticity of a new Ti-based metallic glass matrix composite upon dynamic loading. Materials Science and Engineering: A, 2016, 677: 376–383.
[22] Mandal S, Kailath A J. Enhanced plasticity of Cu-Zr-Ti bulk metallic glass and its correlation with fragility. Metallurgical and Materials Transactions A, 2019, 50: 199–208.
[23] Cheng J L, Chen G, Xu F, et al. Correlation of the microstructure and mechanical properties of Zr-based in-situ bulk metallic glass matrix composites. Intermetallics, 2010, 18(12): 2425–2430.
[24] Chen G, Cheng J L, Liu C T. Large-sized Zr-based bulk-metallic-glass composite with enhanced tensile properties. Intermetallics, 2012, 28: 25–33.
[25] Douglas C H, Jin Y S, Aaron W, et al. Development of tough, low-density titanium-based bulk metallic glass matrix composites with tensile ductility. PNAS, 2008, 105(51): 20136–20140.
[26] Hofmann D C, Suh J Y, Wiest A, et al. Designing metallic glass matrix composites with high toughness and tensile ductility. Nature, 2008, 451(7182): 1085–1089.
[27] Lewandowski J J, Greer A L. Temperature rise at shear bands in metallic glasses. Natural Materials, 2006, 5(1): 15–18.
[28] Zhang T W, Ye H Y, Shi J Y, et al. Dendrite size dependence of tensile plasticity of in situ Ti-based metallic glass matrix composites. Journal of Alloys and Compounds, 2014, 583: 593–597.